AIP | Review of Scientific Instruments

# A cylindrical quadrupole ion trap in combination with an electrospray ion source for gas-phase luminescence and absorption spectroscopy

Mark H. Stockett, Jørgen Houmøller, Kristian Støchkel, Annette Svendsen, and Steen Brøndsted Nielsen

Citation: Review of Scientific Instruments **87**, 053103 (2016); doi: 10.1063/1.4948316
View online: http://dx.doi.org/10.1063/1.4948316
View Table of Contents: http://scitation.aip.org/content/aip/journal/rsi/87/5?ver=pdfcov
Published by the AIP Publishing



# A cylindrical quadrupole ion trap in combination with an electrospray ion source for gas-phase luminescence and absorption spectroscopy

Mark H. Stockett,[a] Jørgen Houmøller, Kristian Støchkel, Annette Svendsen, and Steen Brøndsted Nielsen
*Department of Physics and Astronomy, Aarhus University, Aarhus, Denmark*

(Received 5 February 2016; accepted 16 April 2016; published online 3 May 2016)

A relatively simple setup for collection and detection of light emitted from isolated photo-excited molecular ions has been constructed. It benefits from a high collection efficiency of photons, which is accomplished by using a cylindrical ion trap where one end-cap electrode is a mesh grid combined with an aspheric condenser lens. The geometry permits nearly 10% of the emitted light to be collected and, after transmission losses, approximately 5% to be delivered to the entrance of a grating spectrometer equipped with a detector array. The high collection efficiency enables the use of pulsed tunable lasers with low repetition rates (e.g., 20 Hz) instead of continuous wave (cw) lasers or very high repetition rate (e.g., MHz) lasers that are typically used as light sources for gas-phase fluorescence experiments on molecular ions. A hole has been drilled in the cylinder electrode so that a light pulse can interact with the ion cloud in the center of the trap. Simulations indicate that these modifications to the trap do not significantly affect the storage capability and the overall shape of the ion cloud. The overlap between the ion cloud and the laser light is basically 100%, and experimentally >50% of negatively charged chromophore ions are routinely photodepleted. The performance of the setup is illustrated based on fluorescence spectra of several laser dyes, and the quality of these spectra is comparable to those reported by other groups. Finally, by replacing the optical system with a channeltron detector, we demonstrate that the setup can also be used for gas-phase action spectroscopy where either depletion or fragmentation is monitored to provide an indirect measurement on the absorption spectrum of the ion. *Published by AIP Publishing.* [http://dx.doi.org/10.1063/1.4948316]

## I. INTRODUCTION

Spectroscopy of (bio)molecular chromophore ions isolated *in vacuo* is a field of intense research with the goal to reveal their intrinsic electronic structure in the absence of perturbations from a solvent or protein micro-environment.[1–7] These large and fragile chromophore ions are typically produced by electrospray ionization (ESI) to guarantee a soft transfer to the gas phase. Comparisons of gas-phase spectra to those measured when the chromophore is fully solvated or within a protein pocket provide information on, e.g., the effect of nearby water molecules or amino acid residues. Most work has focused on absorption spectroscopy where absorption is identified indirectly from either ion dissociation or electron detachment, so-called action spectroscopy. This is because the ion density is too low for a traditional transmission experiment where the attenuation of light passing through a sample is measured. Instead, specialized mass spectroscopy equipment is required to identify the fate of the ion after light absorption. Only a few experimental groups have measured the light emitted from mass-selected photoexcited ions. Here we present a new setup to measure luminescence from ions produced by ESI, but first we discuss some of the difficulties associated with such experiments.

In most luminescence spectroscopy experiments on molecular ions produced by ESI, the ions are trapped in either a linear quadrupole trap, a Paul trap (i.e, a 3-D quadrupole trap), or a Penning trap.[8–16] The experiments are non-trivial, not only because of the inherently low ion density but also because photons are emitted in all directions, and the collection of the emitted photons is limited by poor optical access to the trapped ions. Sensitive light detectors are needed to detect each of the rare events. Detection efficiencies are typically much less than 1% of the total emitted photons. As an added complication, light scattered from the laser or ambient light is also detected, which reduces the signal-to-noise ratio, or even causes saturation of the detector if one is not careful enough. The same ions are irradiated multiple times with the use of either high repetition rate (e.g., 80 MHz) pulsed lasers or continuous wave (cw) lasers. This approach necessitates collisional (or radiative) cooling of the excited ions between each excitation event. The pressure of the helium buffer gas used to facilitate the trapping of the ions, together with the applied laser power, are therefore highly important adjustable parameters. The rate of collisions at typical buffer gas densities ($10^{14}$ cm$^{-3}$) is $\sim 10^5$ s$^{-1}$ while the time between two laser pulses from an 80 MHz laser is only 12.5 ns. For a pulsed laser experiment, the number of photons in each pulse has to be kept low to avoid two-photon absorption, which is the reason for the use of high repetition rate lasers. The optimal solution is to produce a high number of photons broadly distributed over time to maximize the number of excitation events, each associated with emitted photons from the ions being hit. A cw laser is as such the best choice but the wavelength tunability is poor compared to that of a pulsed laser. An alternative

[a]Electronic mail: stockett@phys.au.dk

approach, described here, utilizes a laser with a low repetition rate (20 Hz), and where the ion trap is emptied and refilled following every laser shot.

While measuring the spectrum of light emitted (i.e., dispersed fluorescence) from isolated ions is difficult for the above-mentioned reasons, it has some advantages over gas-phase absorption spectroscopy. Unlike action spectroscopy, where the absorption of multiple photons is often required to induce measurable fragmentation, fluorescence can be observed following the absorption of just a single photon. This is particularly important for large molecular ions that are not easily dissociated, and where kinetic shifts can skew the spectrum obtained from an absorption experiment. Indeed, beautiful fluorescence spectra of ionic laser dyes have been reported, and even time-resolved light emission has been followed on the nanosecond time scale.[8,17–19] Spectra have also been published of biomolecular ions, e.g., xanthene-based rhodamine dyes,[11,12,15,19] fluorescein and derivatives,[20,21] and non-covalent host-guest complexes.[17] Finally, Förster Resonance Energy Transfer (FRET) experiments on gas-phase biomolecular ions have been performed[22–31] to monitor the separation of double-stranded oligonucleotide anions (i.e., duplex melting) or conformations of peptides and proteins and noncovalent complexes.

To study molecular ions that are produced by low-current ion sources (e.g., ESI) and that have low fluorescence quantum yields, setups with high collection efficiencies are desirable. Further, such setups are crucial if laser systems with low repetition rates are to be employed. Here we describe a homebuilt setup that is based on a Paul trap with a cylindrical geometry following the design of Wells *et al.*[32] The advantage of using a Paul trap instead of, e.g., a linear quadrupole trap is the confinement of ions to the center, and the light emitted after photo-excitation is almost originating from a point source. The cylindrical variant is much easier to construct and modify than the traditional version which utilizes hyperbolic electrodes. In our design, a hole in the cylindrical electrode permits laser irradiation of the trapped ions and one end-cap electrode is a wire mesh grid. A condenser lens is mounted as close as possible to the grid electrode allowing light collection from a greater solid angle than in other existing setups. We have performed detailed numerical simulations which show that, despite all the modifications, the electric field near the center of our trap is close to that of an ideal quadrupole trap. The idea behind this design is based on a setup made by O'Keefe and co-workers[33–36] to measure light-induced fluorescence spectra of small molecular cations (e.g., $CD^+$, $N_2^+$, and $BrCN^+$) produced directly in a quadrupole ion trap by electron ionization. Applying this approach to larger molecular ions was suggested by Parks and co-workers over a decade ago,[9] but never implemented until now.

We demonstrate that our setup provides high quality dispersed fluorescence spectra of ions produced by ESI even when a 20 Hz laser is used as the excitation source. In contrast to other ESI-trap fluorescence experiments, the ions are only irradiated once before the trap is emptied, and there are therefore no issues with thermalization of photo-excited ions or photodissociation (the latter of course depletes the population of ions stored in the trap and thus lowers the fluorescence signal but the fragment ions do not otherwise disturb the experiment); we will discuss this issue later in this article. The setup can also be used for absorption spectroscopy (based on dissociation and electron detachment) from a simple replacement of the light collection optics with a channeltron detector. Finally, we discuss the potential use of such a setup for detection of light emission from cryogenically cooled ions.

## II. DESIGN

The electrospray ion source and cylindrical quadrupole ion trap, shown together in Fig. 1, are similar to those previously used on the ELISA (Electrostatic Ion Storage Ring, Aarhus) electrostatic storage ring.[37] All components were manufactured in-house. Ions formed by electrospray ionization enter the first vacuum chamber through a heated capillary. A tube lens focuses the ions through a skimmer into a second chamber. The ions are guided through this chamber, which serves mainly as a differential pumping stage, by an octopole ion guide. A lens packet focuses the ions through a small aperture at the exit of the ion guide into a third chamber where the ion trap is mounted. An Einzel lens focuses the ion beam into the entrance aperture of the trap.

The cylindrical ion trap, shown in Fig. 2, was built using the optimized geometry determined by Wells *et al.*[32] The cylindrical geometry combines ease of manufacture with adequate performance in mass-selective operation. The inner radius of the cylinder is $r_1 = 10$ mm and the axial distance from the center of the trap to the end-cap electrode is $z_1 = 9$ mm, and there is a gap of $D = 1$ mm between the cylinder electrode and the end-caps. A radio frequency (RF) potential of frequency $\Omega/2\pi = 770$ kHz and amplitude up to $V = 1.5$ kV (0-peak) is applied to the cylinder using a home built power supply to create an approximate quadrupolar potential for ion trapping. Additional DC voltages ±15 V are applied to the end-caps. A $L = 4$ mm hole through the side of the cylinder electrode permits laser excitation of the trapped ions. The laser pulse

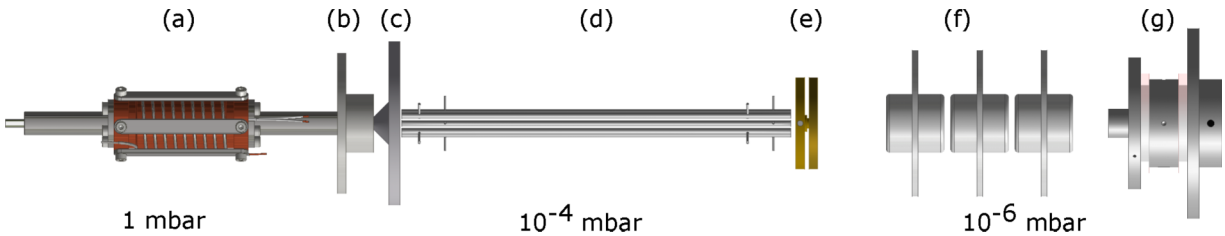


FIG. 1. Schematic of electrospray ion source and cylindrical ion trap. Shown are the (a) heated capillary, (b) tube lens, (c) skimmer, (d) octopole ion guide, (e) lens packet, (f) Einzel lens, and (g) cylindrical ion trap.

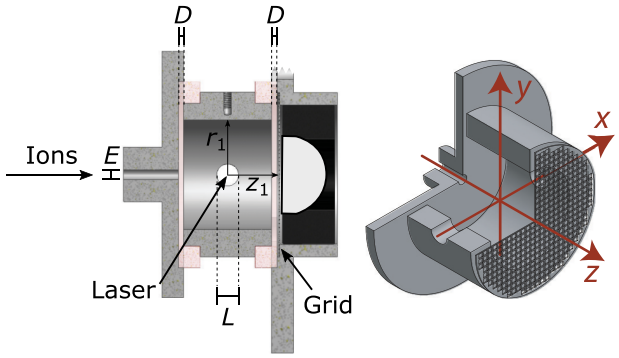


FIG. 2. Cutaway views of the cylindrical ion trap with modified end-cap for fluorescence experiments. A wire mesh grid electrode permits more emitted radiation to be collected by the aspheric condenser lens directly behind the grid. The hole in the cylinder (diameter $L = 4$ mm) allows laser access. Ions enter the trap through a hole of diameter $E = 2$ mm. Also indicated are the trap dimensions $r_1 = 10$ mm, $z_1 = 9$ mm, and the gap between the cylinder and end-cap electrodes $D = 1$ mm. The axes used in our numerical simulations are defined in the right-hand view, where the lens and its mounting have been removed to reveal the grid.

(beam diameter ~3 mm) enters and exits the vacuum chamber containing the trap through anti-reflection coated fused silica windows oriented perpendicular to the beam. No baffles are used to reduce scattered laser light; a simple iris outside the chamber is used to define the beam diameter.

For use in fluorescence experiments, one of the end-caps has been replaced with a wire mesh grid electrode to permit more light to be collected. A schematic of the optical system is shown in Fig. 3. An aspheric condenser lens (Thorlabs, 18 mm diameter) is mounted inside the modified end-cap with the optical surface as close to the grid as possible to maximize the solid angle for light collection. The focal length of the lens (15 mm) is chosen such that the ion cloud sits slightly inside the focal distance. This yields a well-collimated beam of collected radiation which is coupled out of the vacuum chamber through an anti-reflection coated window. The high numerical aperture of the aspheric lens (0.57) corresponds to a solid angle of 1.1 sr, meaning that nearly 10% of the light emitted by the ions falls within the cone of angles collected by the lens. Outside the vacuum chamber, notch filters (Thorlabs) used to reduce scattered laser light and an achromatic focusing lens (Thorlabs, focal length 10 cm) are mounted on a rail

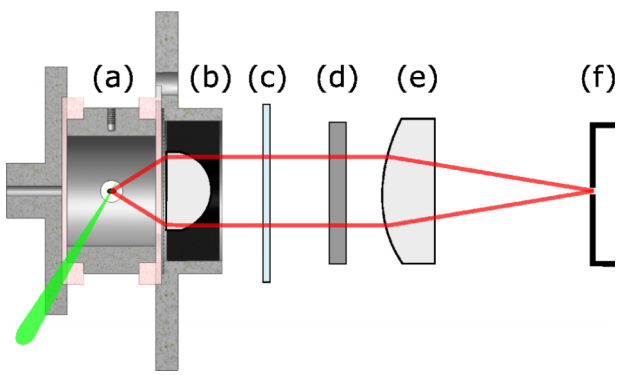


FIG. 3. Schematic optical layout showing (a) trap, (b) condenser lens, (c) chamber window, (d) notch filter, (e) collector lens, and (f) spectrometer entrance slit.

system co-axial with the ion trap. The achromatic lens focuses the collected radiation onto the entrance slit of a grating spectrometer (Andor Shamrock 303i, 303 mm focal length) equipped with an electron multiplying CCD camera (Andor Newton model DU970P-BVF, $1600 \times 200\,16$ $\mu$m $\times$ 16 $\mu$m pixels). Taking into account transmission losses from the grid electrode and all optical elements, we estimate that approximately 5% of the emitted radiation is delivered to the spectrometer entrance slit. This high collection efficiency distinguishes our apparatus from those developed by other groups.

For all fluorescence spectra presented in this article, the 1 MHz readout mode of the CCD camera was used, with a pre-amplifier gain of 4 and an electron multiplication gain of 255. A 50 kHz readout mode was not found to meaningfully improve the signal-to-noise ratio in our experiments. A 300 lines/mm grating (500 nm blaze) and a 1.5-2.0 mm slit width on the spectrometer provided adequate resolution. The triggering of the laser, camera, and trap are controlled using a simple LabVIEW program and a TTL pulse generator.

## III. NUMERICAL SIMULATIONS

To investigate the properties of the cylindrical ion trap with the mesh grid electrode and to estimate the size of the ion cloud, numerical simulations were performed using the SIMION 8.0 software. The program was used to solve the Laplace equation for the chosen trap geometry on a grid with a spatial resolution of 0.1 mm. For the cloud simulations, 1000 ions of mass 163 amu (or 479 amu) and charge $-1e$ (or $+1e$) were initialized in the center of the trap with a kinetic energy of 0.2 eV and a corresponding velocity vector uniformly distributed in all directions. Ion trajectories were computed by numerical integration of the equations of motion while at the same time taking into account collisions between the ion and the He buffer gas. The collisions happened at random times, but such that the average distance travelled by the ions between collisions was equal to the mean free path (assuming a collisional cross section of $\sigma = 2.3 \times 10^{-18}$ m$^2$) at a buffer gas pressure of $5{\times}10^{-3}$ mbar. The collisions were modelled as hard-sphere elastic collisions in which the He atom was generated with a random velocity drawn from a Maxwell-Boltzmann velocity distribution with a temperature of $T = 300$ K (see Ref. 38 for details). Each ion was propagated for a time span of 4000 $\mu$s, and its position was logged at a time interval of 10 $\mu$s, but only during the last 1000 $\mu$s of the simulation to ensure that the ion ensemble was equilibrated. To simulate the stability region, the buffer gas collisions were turned off, and the ions were initialized slightly outside the trap center with a kinetic energy of 2 meV with a spatially isotropic velocity distribution. The RF amplitude (0-peak), $V$, and DC offset, $U$, were varied, and a point in $(V, U)$ space was defined as stable if the ions were still trapped after a propagation time of 1 ms.

Fig. 4 shows the ion column density for two of the ions presented later in this work, simulated under typical experimental conditions. Also indicated is the area accessible to the laser light. The FWHM (Full Width at Half Maximum) of the distributions in the radial and axial directions is

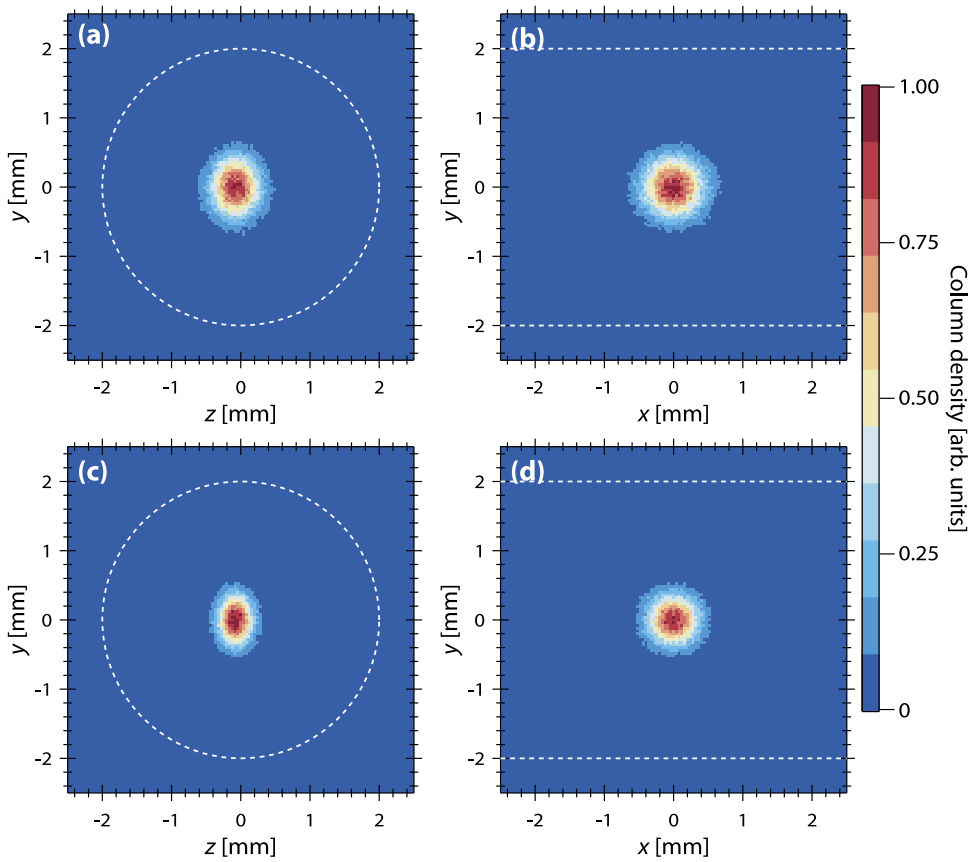


FIG. 4. Simulated column densities of ions in cylindrical trap at a buffer gas pressure of $5\times10^{-3}$ mbar at a temperature of $T = 300$ K. Panels (a) and (b) are for ions of mass 163 amu and charge $q = -1e$ trapped at an RF amplitude of $V = 450$ V and an RF frequency of $\Omega/2\pi = 770$ kHz, and with end-cap potentials of +15 V. The ion cloud is viewed along the $x$ (a) and $z$ (b) axes. Panels (c) and (d) are for ions of mass 479 amu and charge $q = +1e$ trapped at an RF amplitude of $V = 1000$ V and an RF frequency of $\Omega/2\pi = 770$ kHz, and with end-cap potentials of −15 V. The ion cloud is viewed along the $x$ (c) and $z$ (d) axes. The areas bounded by the white dashed curves indicate the areas accessible to the laser light.

0.7 mm and 0.5 mm for ions of mass 163 amu and 479 amu respectively. Hence, both ion clouds occupy a small volume compared to that accessible to the laser light thus ensuring a good overlap between the two.

In Fig. 5, we show the equipotential curves calculated using SIMION for the cylindrical ion trap (full lines). From these simulations, it is clear the that wire mesh grid electrode causes only minor distortions of the field, and only very close

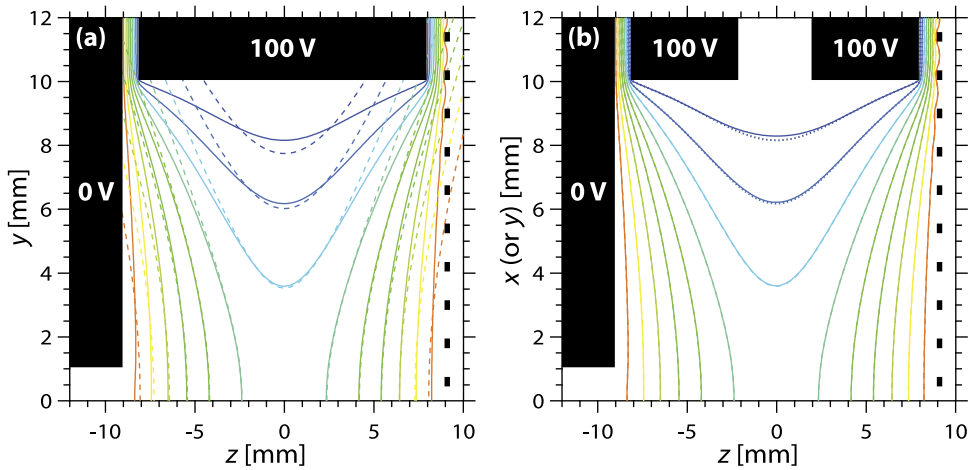


FIG. 5. Calculated equipotential curves of the cylindrical ion trap with a RF potential of 100 V applied to the ring electrode while both end cap electrodes are kept at ground potential. (a) Equipotential curves in the $(z, y)$ plane. The full lines display the equipotential curves in steps of 10 V from 0 V to 100 V. The dashed lines represent the corresponding equipotential curves of the pure quadrupolar potential that provides the best description of the cylindrical trap potential. (b) Equipotential curves in the $(z, x)$ plane. The full lines display the equipotential curves in steps of 10 V from 0 V to 100 V. For comparison, the dotted lines represent the corresponding equipotential curves in the $(z, y)$ plane also shown in (a).

to the grid itself. In Fig. 5(a), an ideal quadrupolar field (dashed lines) is shown for comparison. Although the field in our cylindrical trap deviates from the ideal case close to the electrodes, it is very similar near the center of the trap (recall that the ion cloud diameter is less than 1 mm). In Fig. 5(b), the (very small) effect of the laser access holes can be seen by comparing the equipotential curves in the $(z, x)$ (solid lines, see Fig. 2 for axes) to those in the $(z, y)$ plane (dotted lines, same as solid lines in Fig. 5(a)). Taken together, these simulations demonstrate that our modified cylindrical ion trap should function in much the same way as a traditional Paul trap.

For future experiments, we intend to operate the trap in a mass-selective mode by adding a DC offset $U$ to the RF potential applied to the cylinder electrode, using the octopole as a pre-trap. We have therefore simulated, and present here, the stability diagram for our cylindrical trap, including the effects of the grid electrode and laser access holes. These calculations are also important for establishing the low-mass cutoff in RF-only mode. The stability region of an ideal three-dimensional quadrupole ion trap is described in terms of the $a$ and $q$ parameters defined as[39]

$$a_z = -2a_r = \frac{-16qeU_0}{m(r_0^2 + 2z_0^2)\Omega^2}, \quad (1)$$

$$q_z = -2q_r = \frac{8qeV}{m(r_0^2 + 2z_0^2)\Omega^2}. \quad (2)$$

Here, $m$ and $qe$ are the ion mass and charge, $\Omega$ and $V$ the angular frequency and amplitude of the RF potential, while $U_0 = U - U_{\text{end}}$ is the difference between the static potential applied to the ring electrode, $U$, and that applied to the end cap electrodes, $U_{\text{end}}$. The parameters, $r_0$ and $z_0$, describe the trap geometry such that $2r_0$ is the innermost diameter of the ring electrode while $2z_0$ is the smallest distance between the end cap electrodes (in analogy with our definition of $r_1$ and $z_1$ for the cylindrical ion trap in Fig. 2). In order to apply the well-established theory for ideal quadrupole ion traps to our cylindrical ion trap, a pure quadrupolar potential is fitted to the potential created by the current trap geometry (Fig. 5) which yields the values $r_0 = 9.2$ mm and $z_0 = 8.8$ mm as compared to $r_1 = 10$ mm and $z_1 = 9$ mm. Fig. 6 displays the simulated stability region for two different potentials applied to the end cap electrodes and the theoretical stability regions obtained using the ordinary Mathieu stability diagram with the $a$ and $q$ parameters described above. As can be seen, the theoretical curves provide a very good description of the simulated stability regions. It is also clear that the potential applied to the end cap electrodes must be taken into consideration in mass-selection mode, as this potential offsets the entire stability region. Based on our calculated stability region parameters and the operating range of our RF power supply, we should be able to mass-selectively store ions with masses from about 80 to 270 amu. With no mass-selection, there is in principle no upper limit to the mass of the ion which can be stored.

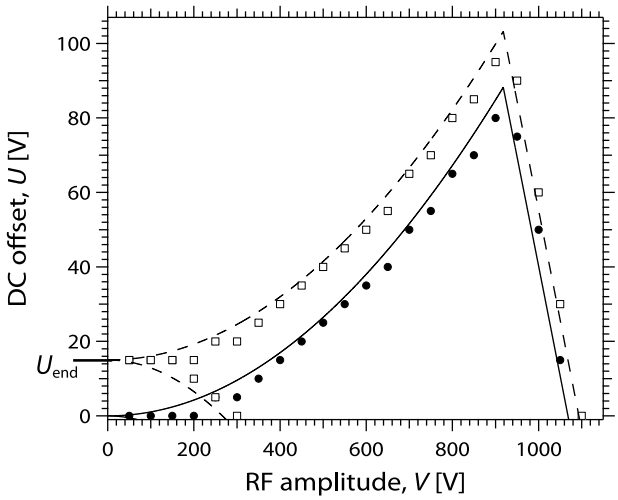


FIG. 6. Simulated stability region for an ion of mass 163 amu in the cylindrical ion trap. The filled circles and open squares represent the simulated stability region with the end cap electrodes kept at ground potential or at +15 V, respectively. Also shown are the two theoretical stability regions determined by use of Eq. (1).

## IV. RESULTS

The fluorescence spectra of three different cations from the family of Rhodamine laser dyes (Rhodamine 6G (479 amu), Rhodamine B (479 amu), and Sulphorhodamine B (559 amu)) recorded with our apparatus are shown in Fig. 7. An optical parametric oscillator pumped with a 20 Hz, frequency-tripled, Q-switched Nd:YAG laser (EKSPLA) produced <10-ns pulses which were overlapped with the stored ion cloud. The linewidth of the laser is <5 $cm^{-1}$, and approximately 0.1 mJ/pulse was delivered to the trap. The ions are accumulated in the trap for approximately 50 ms (one laser cycle time) and then irradiated with a single laser pulse, with the resulting emission being out-coupled and detected as described above. We note that no DC offset was applied to the cylinder electrode ($U = 0$), and thus all ions produced in the ESI source with masses greater than the low mass cutoff (about 160 amu for the RF amplitude used, $V = 1000$ V) were stored. The trap is then emptied by switching off the RF trapping voltage and raising the entrance end-cap voltage

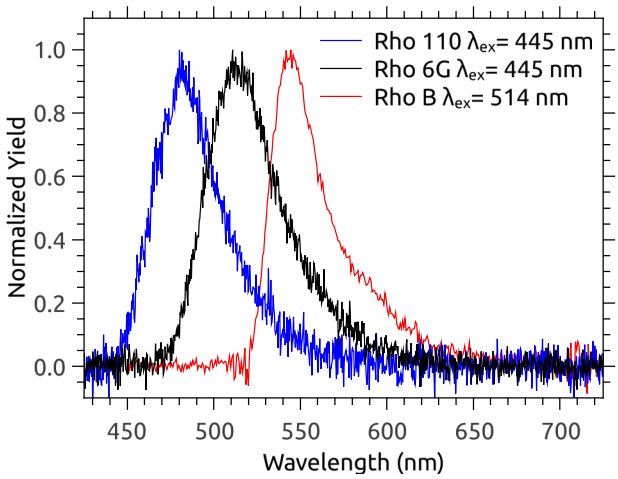


FIG. 7. Dispersed fluorescence spectra of trapped Rhodamine 110, Rhodamine 6G, and Rhodamine B cations excited by a ns-pulsed laser at the indicated wavelengths. Notch filters at corresponding wavelengths were used to reduce scattered laser light.

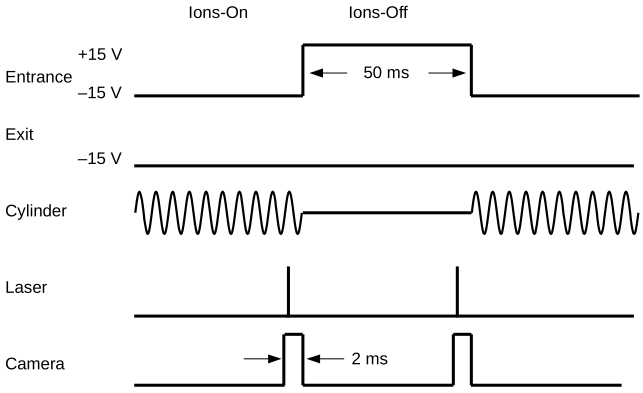


FIG. 8. Timing diagram for measuring fluorescence spectra of positive ions with a 20 Hz ns-pulsed laser.

to +15 V. Another spectrum is then acquired after the next laser shot with no ions in the trap (laser-on, ions-off). The +15 V entrance end-cap voltage prevents ions from entering the trap during the ions-off acquisition. A schematic timing diagram for one such cycle is shown in Fig. 8. This cycle is repeated with alternating acquisitions of ions-on and ions-off spectra to improve signal-to-noise. The spectra in Fig. 7 are the difference between the ions-on and ions-off signals accumulated over 10 000 cycles (about 15 min).

Dispersed fluorescence spectra of Rhodamine B cations were measured with different helium buffer gas pressures in the trap, varying by more than an order of magnitude (Fig. 9). The pressure is not measured directly in the trap for technical reasons, and the gauge reading is therefore a lower bound on the actual trap pressure. Further, these values have not been corrected for gas species. The lowest value was $0.5 \times 10^{-4}$ mbar and the highest $8.0 \times 10^{-4}$ mbar. While the total fluorescence signal not surprisingly depends on pressure as there is an optimum pressure for ion trapping, the normalized dispersed fluorescence spectra do not. This clearly shows the advantage of replacing ions between each laser irradiation event. We do not rely on collisional cooling of hot ions, which is needed when the same ions are irradiated (quasi-)continuously.[10,12]

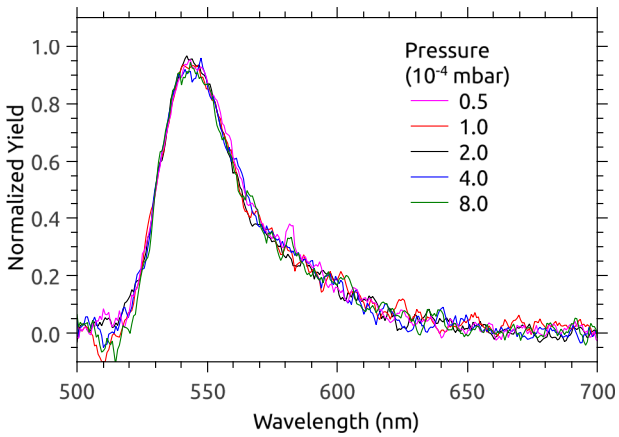


FIG. 9. Dispersed fluorescence spectra of Rhodamine B cations ($\lambda_{ex}$ = 514 nm, 250 $\mu$J/pulse) recorded at different buffer gas pressures (measured outside the trap).

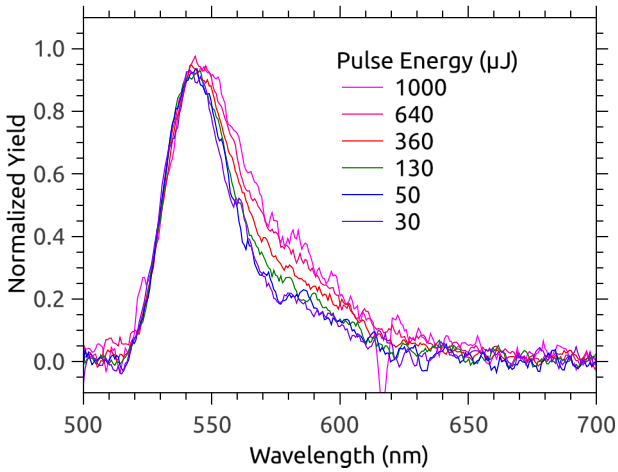


FIG. 10. Dispersed fluorescence spectra of Rhodamine B cations ($\lambda_{ex}$ = 514 nm) recorded at different laser intensities (measured following the trap).

It should be noted that by using a high-intensity pulsed laser, multiple photon absorption is possible within a single pulse. This distorts the shape of the fluorescence band, as shown in Fig. 10. Use of high laser pulse energies (measured using a power meter placed after the trap) introduces a shoulder to the red, but the band maximum remains unchanged.

We have also used our setup to measure the fluorescence spectra of ions excited with a continuous wave (cw) laser. In Fig. 11, we show the results of one such experiment, where Rhodamine 110 cations were excited using a blue (405 nm) laser pointer. For these measurements, the camera exposure time was increased to 40 ms, but all other timing parameters (Fig. 8) were kept the same. This measurement demonstrates the sensitivity and flexibility of our apparatus.

To obtain reasonable signal-to-noise ratios for the fluorescence spectra of laser dyes using our pulsed laser, acquisition times of minutes are needed. Hence it takes at least an order of magnitude longer time to record a spectrum with a 20-Hz laser than it does when much higher repetition rate lasers or cw lasers are used. However, our approach has several advantages: (1) The photon collection efficiency is higher than that for other

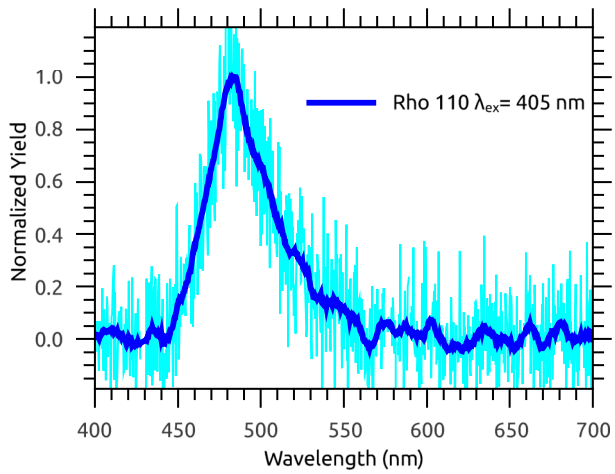


FIG. 11. Dispersed fluorescence spectrum of trapped Rhodamine 110 cations excited with a 5 mW, 405 nm cw laser.

setups where fluorescence is measured from ions produced by ESI. (2) Fluorescence spectra are independent of helium buffer gas pressure as discussed above. (3) The number of photons emitted is directly related to the fluorescence quantum yield and does not change between each laser shot. Hence the time it takes to record a given number of photons emitted from a cloud of trapped ions is linearly proportional to the fluorescence quantum yield. If we assume 100% fluorescence quantum yields for the laser dyes studied, it would take 100 times longer to detect the same number of photons from ions that have a quantum yield of say only 1%. This is a doable experiment. (4) If electron detachment or prompt dissociation occur with a certain probability ($P_{loss}$), the number of ions, $N(n)$, in a multiple irradiation experiment quickly decreases with the number of laser shots ($n$): $N(n) = N_0(1 - P_{loss} \cdot P_{abs})^n$. Here, $N_0$ is the initial number of ions in the trap, and $P_{abs}$ is the probability with which the ion absorbs a photon, which depends on the laser power and can be as high as 50% in our experiments (see Section V). Even if $P_{loss} \cdot P_{abs}$ is only 1%, $N$ is reduced by more than four orders of magnitudes after $n = 1000$ laser shots, that is after only about 10 $\mu$s using a 80 MHz laser. This issue is irrelevant with our setup as long as the fluorescence quantum yield is non-zero. (5) The replacement of ions between each laser shot could be important for further development of a setup for detecting fluorescence from cryogenically cooled ions. Here cooling times between irradiation events become more crucial, which is an issue that is avoided with a low repetition rate. In such experiments, the octupole ion guide in our ESI source could be used as a pre-trap to maximize the cooling time in the Paul trap, an approach that has been demonstrated previously.[40]

## V. DEPLETION MEASUREMENTS

In order to optimize the trapping parameters and laser-ion overlap, we performed photo-depletion measurements on several molecular anions. These experiments also demonstrate the possibilities for utilizing our apparatus for absorption action spectroscopy. For these measurements, the condenser lens and optical assembly is removed and a channeltron detector placed outside the trap facing the grid electrode. While being continuously filled with ions from the electrospray source, the trap is emptied at a repetition rate of 40 Hz. This is accomplished by switching off the RF voltage ($1/e$ fall-time ~3 $\mu$s) and swapping the polarity of the DC voltage on the entrance end-cap from +15 V to −15 V (for negative ions) while keeping the exit end-cap at +15 V. Prior to every

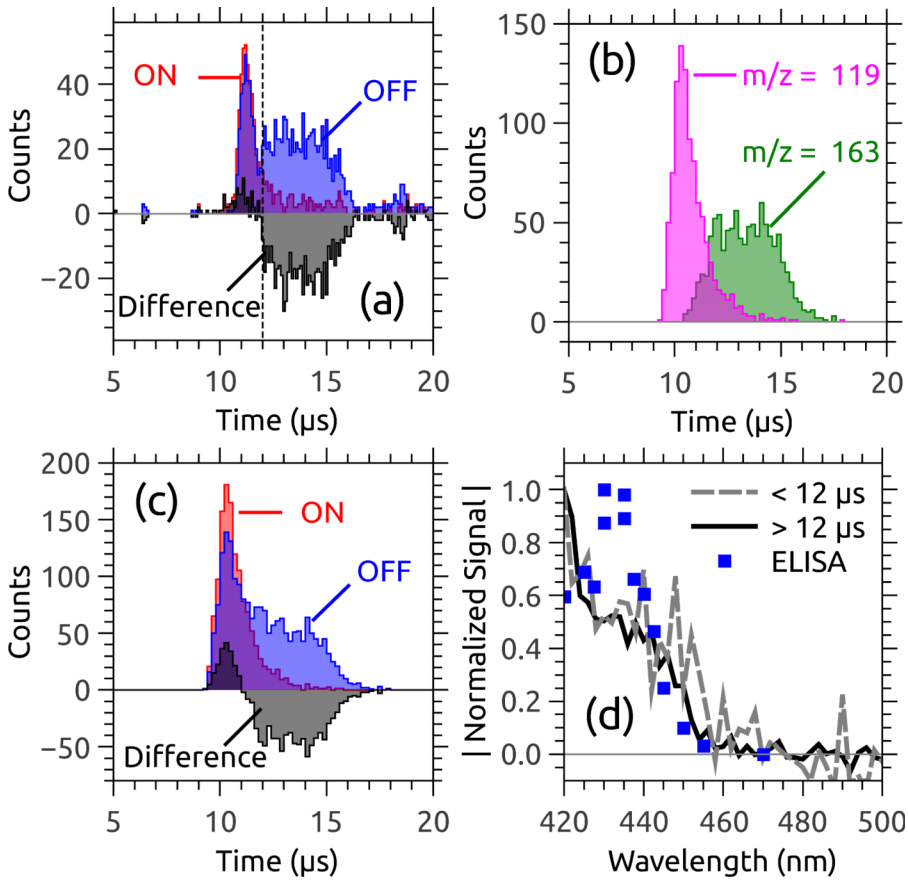


FIG. 12. Action spectroscopy of $pCA^-$ ions stored in the trap. Panel (a) shows the time profiles of the ion bunches ejected from the trap with (ON, red) and without (OFF, blue) laser irradiation, and the difference between the ON and OFF signals (Difference, black) showing clear evidence for photodepletion of the stored $pCA^-$ ions. For times >12 $\mu$s the difference signal is negative indicating electron detachment, whereas for times <12 $\mu$s the difference signal is positive, suggesting fragmentation of the $pCA^-$ ions. Panel (b) shows simulated time profiles for 1000 ions of mass 163 amu ($pCA^-$, green) and 119 amu ($[pCA\text{-}CO_2]^-$, pink) stored in the trap using the same parameters as the experiment. Panel (c) are hypothetical ON, OFF and difference profiles (same labelling as (a)) based on the simulated time profiles in (b). Panel (d) shows the normalized magnitude of the experimental difference signal as a function of excitation wavelength for times >12 $\mu$s (black) and <12 $\mu$s (gray). Also shown are action spectra recorded at the ELISA storage ring.[42]

second emptying, the ion cloud is irradiated with a single laser pulse. The neutralization of the stored anions, whether by direct electron detachment or delayed emission, gives rise to a difference in the number of ions counted by the channeltron between the laser-on and laser-off measurements.

This difference signal can be clearly seen in Fig. 12(a), where we show the ion bunch profiles for deprotonated *trans-p*-coumaric acid ($pCA^-$) ejected from the trap with and without 422 nm laser excitation prior to extraction. The difference signal is negative for times (measured from when the trigger signal to empty the trap is sent) greater than 12 $\mu$s, due to photodepletion of the $pCA^-$ ions. The depletion at this wavelength is greater than 50% of the stored ion population, implying excellent overlap of the laser beam with the ion cloud. The large peak in the time profile between 10 and 12 $\mu$s is presumably due to the presence in the trap of ions other than $pCA^-$ (no mass-selection was applied in these experiments) which are not depleted by irradiation at these wavelengths. Indeed, the difference signal for times <12 $\mu$s is slightly positive, suggesting that these co-stored ions could be charged fragments of $pCA^-$. Time-resolved photodissociation experiments[41] have found that 70% of photo-excited $pCA^-$ ions (mass 163 amu) decay by vibrational auto-detachment, with the rest undergoing dissociation, losing a $CO_2$ group and yielding a fragment with a mass of 119 amu. In Fig. 12(b), we show time profiles simulated in SIMION using the same trapping parameters as in the experiment, but assuming that only ions of mass 163 or 119 amu were stored. Fig. 12(c) shows hypothetical laser-on, laser-off, and difference signals assuming equal initial populations of mass 163 and 119, 100% depletion of mass 163 with 30% fragmentation to mass 119. The agreement with the measured time profiles is striking, and strongly suggests that the difference in time profiles can be viewed as a crude time-of-flight mass spectrum. Fig. 12(d) shows the magnitude of the $pCA^-$ depletion signal (for times >12 $\mu$s) and the positive difference signal (formation of fragments with mass 119 amu, times <12 $\mu$s) as functions of the laser wavelength, corrected for laser power and normalized to the signal at 420 nm. The spectra are identical, and in good agreement with earlier gas-phase absorption spectra measured using the electrostatic storage ring ELISA.[42] While far from definitive, these preliminary results point to exciting possibilities for combining photo-induced dissociation mass spectroscopy experiments with fluorescence measurements using this apparatus.

Another example demonstrating the versatility of our apparatus is shown in Fig. 13, where we show action spectra for deprotonated *trans*-thiophenyl-*p*-coumarate ($pCT^-$) ions. In this case, photo-excitation has been shown to lead to the fast (100 ns timescale) loss of the thiophenyl group with a high Kinetic Energy Release (KER).[41] In our experiments, this high KER causes the fragments to no longer be stored. These fragments are ejected from the trap shortly after the laser pulse in characteristic microbunches in phase with the RF voltage, as shown in the inset of Fig. 13. The two action spectra, measured by monitoring the depletion of the stored $pCT^-$ ions and the ejection of fragment ions, are both in good agreement with previous measurements at ELISA.[42]

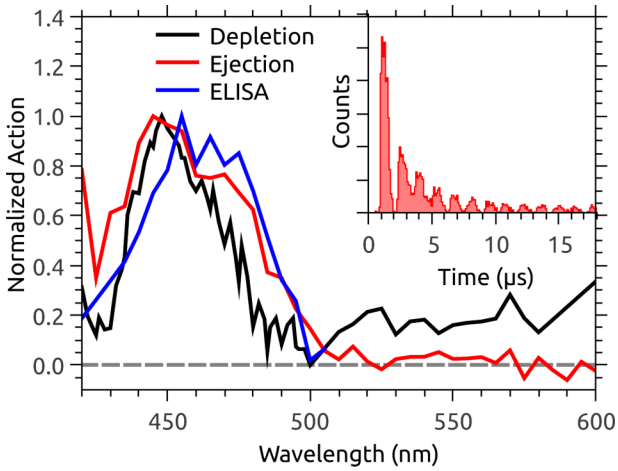


FIG. 13. Action spectra for the $pCT^-$ ion stored in the trap. The action spectrum recorded at the ELISA storage ring is also shown for comparison. The inset shows the ejection of high kinetic energy fragments from the trap in phase with the RF trapping voltage.

## VI. CONCLUSION

We have presented a thorough description of our home-built apparatus for measuring luminescence spectra of trapped molecular ions produced by electrospray ionization (ESI). Our design is based on a modified Paul trap with a cylindrical geometry and a specially designed end-cap for efficient light collection using a condenser lens mounted as close as possible to the emitting ions. The high collection efficiency of our setup permits the use of a low repetition rate (20 Hz) laser for excitation, allowing the trap to be emptied and refilled between each laser shot. In this way, the ions are only irradiated once, eliminating the considerations surrounding the cooling ions between excitation events and the buildup of photoproducts that can occur under continuous irradiation. We have furthermore demonstrated that our setup can be used to measure the absorption spectra of trapped ions. We refer to the apparatus as LUNA, or luminescence instrument in Aarhus, after the latin name for the Moon, which lights up the night sky.

## ACKNOWLEDGMENTS

We gratefully acknowledge support from the Carlsberg Foundation (Grant No. 2013_01_0180), the Villum Foundation, the Danish Council for Independent Research (Grant No. 4181-000488), and the Lundbeck Foundation. The authors also thank Henrik B. Pedersen for technical support in connection with our numerical simulations.

[1]S. Brøndsted Nielsen and J. A. Wyer, *Photophysics of Ionic Biochromophores* (Springer, 2013).
[2]S. M. Wellman and R. A. Jockusch, J. Phys. Chem. A **119**, 6333 (2015).
[3]G. Féraud, M. Berdakin, C. Dedonder, C. Jouvet, and G. A. Pino, J. Phys. Chem. B **119**, 2219 (2014).
[4]F. Rosu, V. Gabelica, E. De Pauw, R. Antoine, M. Broyer, and P. Dugourd, J. Phys. Chem. A **116**, 5383 (2012).
[5]J. C. Marcum, A. Halevi, and J. M. Weber, Phys. Chem. Chem. Phys. **11**, 1740 (2009).
[6]J. Rajput, D. B. Rahbek, L. H. Andersen, A. Hirshfeld, M. Sheves, P. Altoè, G. Orlandi, and M. Garavelli, Angew. Chem., Int. Ed. **49**, 1790 (2010).

[7]S. Brøndsted Nielsen, M. Brøndsted Nielsen, and A. Rubio, Acc. Chem. Res. **47**, 1417 (2014).
[8]J. Friedrich, J. Fu, C. L. Hendrickson, A. G. Marshall, and Y.-S. Wang, Rev. Sci. Instrum. **75**, 4511 (2004).
[9]J. T. Khoury, S. E. Rodriguez-Cruz, and J. H. Parks, J. Am. Soc. Mass Spectrom. **13**, 696 (2002).
[10]N. A. Sassin, S. C. Everhart, B. B. Dangi, K. M. Ervin, and J. I. Cline, J. Am. Soc. Mass Spectrom. **20**, 96 (2009).
[11]M. W. Forbes and R. A. Jockusch, J. Am. Soc. Mass Spectrom. **22**, 93 (2011).
[12]Q. Bian, M. W. Forbes, F. O. Talbot, and R. A. Jockusch, Phys. Chem. Chem. Phys. **12**, 2590 (2010).
[13]M. Kordel, D. Schooss, C. Neiss, L. Walter, and M. M. Kappes, J. Phys. Chem. A **114**, 5509 (2010).
[14]J.-F. Greisch, M. E. Harding, M. Kordel, W. Klopper, M. M. Kappes, and D. Schooss, Phys. Chem. Chem. Phys. **15**, 8162 (2013).
[15]K. Chingin, R. M. Balabin, V. Frankevich, H. Chen, K. Barylyuk, R. Nieckarz, A. Fedorov, and R. Zenobi, Phys. Chem. Chem. Phys. **12**, 14121 (2010).
[16]K. Chingin, H. Chen, G. Gamez, and R. Zenobi, J. Am. Soc. Mass Spectrom. **20**, 1731 (2009).
[17]M. F. Czar and R. A. Jockusch, ChemPhysChem **14**, 1138 (2013).
[18]A. M. Nagy, F. O. Talbot, M. F. Czar, and R. A. Jockusch, J. Photochem. Photobiol., A **244**, 47 (2012).
[19]S. K. Sagoo and R. A. Jockusch, J. Photochem. Photobiol., A **220**, 173 (2011).
[20]P. D. McQueen, S. Sagoo, H. Yao, and R. A. Jockusch, Angew. Chem., Int. Ed. **49**, 9193 (2010).
[21]H. Yao and R. A. Jockusch, J. Phys. Chem. A **117**, 1351 (2013).
[22]A. S. Danell and J. H. Parks, Int. J. Mass Spectrom. **229**, 35 (2003).
[23]M. Dashtiev, V. Azov, V. Frankevich, L. Scharfenberg, and R. Zenobi, J. Am. Soc. Mass Spectrom. **16**, 1481 (2005).
[24]F. O. Talbot, A. Rullo, H. Yao, and R. A. Jockusch, J. Am. Chem. Soc. **132**, 16156 (2010).
[25]A. T. Iavarone and J. H. Parks, J. Am. Chem. Soc. **127**, 8606 (2005).
[26]A. T. Iavarone, A. Patriksson, D. van der Spoel, and J. H. Parks, J. Am. Chem. Soc. **129**, 6726 (2007).
[27]A. T. Iavarone, D. Duft, and J. H. Parks, J. Phys. Chem. A **110**, 12714 (2006).
[28]A. T. Iavarone, J. Meinen, S. Schulze, and J. H. Parks, Int. J. Mass Spectrom. **253**, 172 (2006).
[29]X. Shi and J. H. Parks, J. Am. Soc. Mass Spectrom. **21**, 707 (2010).
[30]X. Shi, D. Duft, and J. H. Parks, J. Phys. Chem. B **112**, 12801 (2008).
[31]M. F. Czar, F. Zosel, I. König, D. Nettels, B. Wunderlich, B. Schuler, A. Zarrine-Afsar, and R. A. Jockusch, Anal. Chem. **87**, 7559 (2015).
[32]J. M. Wells, E. R. Badman, and R. G. Cooks, Anal. Chem. **70**, 438 (1998).
[33]F. J. Grieman, B. H. Mahan, and A. O'Keefe, J. Chem. Phys. **72**, 4246 (1980).
[34]F. J. Grieman, B. H. Mahan, A. O'Keefe, and J. S. Winn, Faraday Discuss. **71**, 191 (1981).
[35]B. H. Mahan and A. O'Keefe, J. Chem. Phys. **74**, 5606 (1981).
[36]F. J. Grieman, B. H. Mahan, and A. O'Keefe, J. Chem. Phys. **74**, 857 (1981).
[37]J. U. Andersen, P. Hvelplund, S. Brøndsted Nielsen, S. Tomita, H. Wahlgreen, S. P. Møller, U. V. Pedersen, J. S. Forster, and T. J. D. Jørgensen, Rev. Sci. Instrum. **73**, 1284 (2002).
[38]A. D. Appelhans and D. A. Dahl, Int. J. Mass Spectrom. **216**, 269 (2002).
[39]R. E. March and J. F. Todd, *Quadrupole Ion Trap Mass Spectrometry* (John Wiley & Sons, 2005), Vol. 165.
[40]J. A. Wyer and S. Brøndsted Nielsen, Angew. Chem., Int. Ed. **51**, 10256 (2012).
[41]L. Lammich, J. Rajput, and L. H. Andersen, Phys. Rev. E **78**, 051916 (2008).
[42]I. B. Nielsen, S. Boyé-Péronne, M. O. A. El Ghazaly, M. B. Kristensen, S. Brøndsted Nielsen, and L. Andersen, Biophys. J. **89**, 2597 (2005).